Journal of Inflammation Research

Dovepress
open access to scientific and medical research

Open Access Full Text Article

ORIGINAL RESEARCH

Rosmarinic Acid Alleviates Radiation-Induced Pulmonary Fibrosis by Downregulating the tRNA N7-Methylguanosine Modification-Regulated Fibroblast-to-Myofibroblast Transition Through the Exosome Pathway

Tingting Zhang[1–3,*], Jinglin Mi[1–3,*], Xinling Qin[1–3,*], Zhechen Ouyang[1–3], Yiru Wang[1–3], Zhixun Li[1–3], Siyi He[1–3], Kai Hu[1–3], Rensheng Wang[1–3], Weimei Huang[1–3]

[1]Department of Radiation Oncology, the First Affiliated Hospital of Guangxi Medical University, Nanning, Guangxi, People's Republic of China; [2]Guangxi Key Laboratory of Immunology and Metabolism for Liver Diseases, Nanning, Guangxi, People's Republic of China; [3]Key Laboratory of Early Prevention and Treatment for Regional High-Frequency Tumors (Guangxi Medical University), Ministry of Education, Nanning, Guangxi, People's Republic of China

*These authors contributed equally to this work

Correspondence: Weimei Huang; Rensheng Wang, Department of Radiation Oncology, the First Affiliated Hospital of Guangxi Medical University, Nanning, Guangxi, People's Republic of China, Email huangweimei@gxmu.edu.cn; wangrensheng@gxmuhospital.cn

Background: Radiation-induced pulmonary fibrosis (RIPF) is a common complication after radiotherapy in thoracic cancer patients, and effective treatment methods are lacking. The purpose of this study was to investigate the protective effect of rosmarinic acid (RA) on RIPF in mice as well as the mechanism involved.

Methods: m7G-tRNA-seq and tRNA-seq analyses were conducted to identify m7G-modified tRNAs. Western blotting, immunohistochemistry, northwestern blotting, northern blotting, immunofluorescence, wound-healing assays and EdU experiments were performed to explore the molecular mechanism by which RA regulates fibroblast-to-myofibroblast transformation (FMT) by affecting the exosomes of lung epithelial cells. Ribo-seq and mRNA-seq analyses were used to explore the underlying target mRNAs. Seahorse assays and immunoprecipitation were carried out to elucidate the effects of RA on glycolysis and FMT processes via the regulation of 6-phosphofructo-2-kinase/fructose-2,6-biphosphatase 3 (PFKFB3) acetylation.

Results: We found that RA had an antifibrotic effect on the lung tissues of RIPF model mice and inhibited the progression of FMT through exosomes derived from lung epithelial cells. Mechanistically, RA reduced the transcription and translation efficiency of sphingosine kinase 1 in lung fibroblasts by decreasing N7-methylguanosine modification of tRNA, downregulating the expression of tRNAs in irradiated lung epithelial cell-derived exosomes, and inhibiting the interaction between sphingosine kinase 1 and the N-acetyltransferase 10 protein in fibroblasts. Furthermore, the acetylation and cytoplasmic translocation of PFKFB3 were reduced by exosomes derived from irradiated lung epithelial cells, which following RA intervention. This suppression of the FMT process, which is triggered by glycolysis, and ultimately decelerating the progression of RIPF.

Conclusion: These findings suggest that RA is a potential therapeutic agent for RIPF.

Keywords: rosmarinic acid, exosomes, tRNA, N7-methylguanosine, radiation-induced pulmonary fibrosis

Introduction

Thoracic cancer is one of the most common malignancies. Radiation therapy is typically necessary for patients with locally advanced chest tumors who are not suitable to undergo surgery or have high-risk factors after surgery often require. However, radiation-induced lung injury (RILI) and fibrosis are crucial factors that restrict the dose and efficacy

Received: 27 March 2024
Accepted: 10 August 2024
Published: 22 August 2024

of radiotherapy. The early manifestation of RILI is radiation-induced pneumonia, and approximately 9–30% of patients gradually develop radiation-induced pulmonary fibrosis (RIPF) after 6 months.[1] RIPF is characterized by irreversible destruction of normal lung tissue structure and deterioration of lung function. Despite of the widespread use of precision radiotherapy techniques, including stereotactic body radiation therapy and intensity-modulated radiotherapy, in clinical practice, the incidence of RIPF remains high. Currently, there is currently a lack of effective treatment plans. Therefore, it is crucial to find effective drugs that are associated with low toxicity for the treatment of RIPF.

Recently, the use of traditional Chinese medicine for the prevention and treatment of pulmonary fibrosis has received considerable attention. Liu et al reported that curcumin inhibited TGF-β2-induced lung fibroblast-to-myofibroblast differentiation and suppressed pulmonary fibrosis by reducing the activity of MMP-9.[2] Emodin not only suppressed the expression of α-SMA, collagen IV, and fibronectin in human embryo lung fibroblasts exposed to TGF-β1 but also the activation of Smad2/3 and STAT3, thus blocking the differentiation of myofibroblasts and the deposition of extracellular matrix.[3] Rosmarinic acid (RA) is a polyphenolic compound isolated from the rosemary plant, which is a member of the Labiatae family.[4] RA exhibits obvious anti-inflammatory and antifibrotic effects on enteritis, osteoarthritis, liver fibrosis, etc.[5] Hsieh et al reported that RA treatment reduced the levels of α-SMA, collagen I, and fibronectin in NRK-52E kidney cells and decreased renal interstitial fibrosis by inhibiting phosphorylated AKT-mediated epithelial-mesenchymal transition in vitro and in vivo.[6] Another study revealed that RA regulated the AMPKα/Smad3 signaling axis to reduce the extent of cardiac fibrosis caused by long-term arterial pressure overload and delayed cardiac remodeling.[7] Similarly, two prior investigations reported by our research group revealed that RA has a protective effect on radiation-induced tissue inflammation and fibrosis. On the one hand, RA downregulated the expression of TNF-α and IL-6 by inhibiting the N-terminal kinase activity of p53/Jun, reduced the oxidative stress response and the apoptosis of parotid gland cells, and ultimately alleviated the radiation-induced parotid gland fibrosis.[8] On the other hand, RA reduced RhoA/ROCK and NF-κB phosphorylation levels by inhibiting MYPT1 expression, there by suppressing the progression of RIPF in rats.[9] Nevertheless, the mechanism by which RA slows radiation-induced tissue fibrosis needs to be further explored.

The fibroblast-to-myofibroblast transition (FMT) is a critical feature of fibrosis after RILI.[10] After radiation, pulmonary fibroblasts transform into myofibroblasts.[11] Myofibroblasts constitute the main source of extracellular matrix, which promotes the formation and development of RIPF.[12] Chemokines, exosomes, and secretory proteins are communication signals that play a crucial role in regulating the redifferentiation of lung fibroblasts by other cells in lung tissue.[13,14] In the prior study, we conducted that RA alleviated the development of RIPF in mice by inhibiting the progression of FMT. Further exploration has revealed that radiation-exposed epithelial cells can promote FMT through the exosome pathway, whereas RA can counteract the effects of irradiated lung epithelial cells on lung fibroblasts. Mechanistically, RA suppressed the METTL1/WDR4-mediated transfer of the ribonucleic acid (tRNA) N7-methylguanosine (m7G) modification in the exosomes of radiation-exposed lung epithelial cells, thereby increasing the translation efficiency and protein expression of the target gene sphingosine kinase 1 (SPHK1). The regulation of SPHK1 in lung fibroblasts is dependent on tRNA m7G modification through the exosome pathway. Moreover, RA suppressed the acetylation of 6-phosphofructo-2-kinase/fructose-2,6-biphosphatase 3 (PFKFB3) in the nucleus and decreased the level of phosphorylated PFKFB3 in the cytoplasm, ultimately reducing FMT triggered by glycolysis in lung fibroblasts. Our findings provide novel therapeutic targets for RIPF as well as insights into its molecular pathophysiology.

Materials and Methods

Animals and Treatments

Eighteen male C57BL/6 mice (7 weeks of age) were obtained from SipeiFu Biotechnology Co., Ltd. (Beijing, China). The mice were randomly divided into three groups: the control (Ctrl) group, irradiation (IR) group and rosmarinic acid plus irradiation (RA+IR) group. The chest regions of the mice in the IR group and the RA+IR group received a single dose of 15 Gy (Varian, California, USA), and the remaining body parts were shielded. RA was purchased from MedchemExpress (New Jersey, USA) and orally administered from 7 days (1 mg/g/day) before irradiation to 24 weeks after irradiation, while the mice in the Ctrl and IR groups were administered saline. The animal experiments were approved by the First Affiliated Hospital of Guangxi Medical University Ethical Review Committee (Approval

Number: 2023-E578-01). All the experimental procedures were rigorously conducted in strict adherence to the ethical guidelines outlined in the Laboratory Animal Welfare Ethical Review Standards of the People's Republic of China (GB/T 35892–2018), ensuring compliance with the highest ethical and scientific standards.

RNA Extraction and Quantitative Real-Time PCR (qRT–PCR)

Total ribonucleic acid (RNA) was extracted with TRIzol reagent (Invitrogen, USA) according to the manufacturer's instructions, after which the concentration and quality of the RNA were measured. Total RNA was reverse transcribed into cDNA with the PrimeScript RT reagent kit with gDNA Eraser (TaKaRa, Japan). qPCR was conducted to evaluate the mRNA levels via the SYBR Green method. The expression levels of genes were normalized to that of GAPDH and quantified via the $2^{-\Delta\Delta}$CT method. The primer sequences were: ACTIN (forward: GTGCTATGTTGCTCTAGACTTCG; reverse: ATGCCACAGGATTCCATACC), METTL1 (forward: CTGTGGCTATGGTGGCTTGT; reverse: TGTTTCATGGCGTTACTTCG), WDR4 (forward: TGAAGAAGAAGCGGCAAAGG; reverse: GGATGAACCAGGGAGGAGGA) and SPHK1 (forward: TCCTGGTATGGGAGGTTATTTC; reverse: AGGGCTCTACTGGGGATGTT).

Western Blotting

The cells were lysed with RIPA lysis buffer, a BCA protein assay kit was used to measure the protein concentration (Beyotime, China). The proteins were separated via SDS–PAGE and transferred to polyvinylidene difluoride membranes. Then, 5% skim milk in Tris-buffered saline containing 0.1% Tween-20 was used to block the proteins for 1 h at room temperature, and the membranes were incubated with primary antibodies (1:1000) overnight at 4 °C. The membranes were incubated with secondary antibodies (1:5000) for 1 h at room temperature. Enhanced chemiluminescence reagent was used to detect the protein signals. The following antibodies were used: METTL1 polyclonal antibody (Proteintech, 14994-1-AP), rabbit anti-WDR4 polyclonal antibody (Absin, abs152662), SPHK1 polyclonal antibody (Proteintech, 10670-1-AP), N-acetyltransferase 10 (NAT10) polyclonal antibody (Proteintech; 13365-1-AP), acetyl-lysine (Affinity, DF7729), PFKFB3 antibody (Affinity, DF12016), phospho-PFKFB3 (Ser461) antibody (Affinity, AF3581), phospho-AMPK alpha (Thr172) antibody (Affinity, AF3423), AMPK alpha antibody (Affinity, AF6423), and ACTIN antibody (Proteintech, 81115-1-RR).

Cell Lines, Transfection and Intervention

The mouse lung epithelial cell lines, TC-1 and MLE-12, were meticulously preserved within our laboratory facilities at the First Affiliated Hospital of Guangxi Medical University,[15] and the processing was approved by the First Affiliated Hospital of Guangxi Medical University (Approval Number: 2023-E578-01). MLFs were purchased from Saios (CL-101m, Wuhan, China). The cells were cultured in DMEM supplemented with 10% fetal bovine serum and 100 U/mL penicillin streptomycin in a 37 °C incubator with 5% CO_2. The cells were digested with 0.25% trypsin every 2–3 days.

When the cells reached approximately 80% confluence, siRNAs and plasmids was transfected into the cells by using Lipofectamine 3000 (Invitrogen, USA). METTL1 and WDR4 overexpression plasmids and METTL1 and WDR4 siRNAs were generated by GenePharma (Shanghai, China). The sequences of siRNAs were: siNC (sense: UUCUCCGAACGUGUCACGUTT), siMETTL1 (sense: GCUUUACCCAGAGUUCUUUTT), siWDR4 (sense: GAGUCCUGAUGACCAGUUUTT).

TC-1 cells and MLE-12 cells were divided into Ctrl, IR and RA+IR groups. TC-1 and MLE-12 cells were pretreated with RA (150 μM) 24 h prior to irradiation in both RA groups. A single dose of 4 Gy X-rays was delivered at a rate of 400 cGy/min to the TC-1 and MLE-12 cells in all the irradiation groups.

Extraction of Exosomes

The cell supernatants were subsequently centrifuged at 10,000 ×g for 45 min at 4 °C to discard the larger vesicles. The supernatants were extracted and filtered through a 0.45 μm filter and then centrifuged for 70 min at 10,000 ×g again and 4 °C and resuspended in PBS. After the removal of the supernatants, the samples were resuspended in 100 μL of PBS. Some exosomes (20 μL) were used for electron microscopy analysis, some (10 μL) were used for particle size analysis, and the remaining exosomes were stored at −80 °C.

EdU Incorporation and Staining

The EdU assay was performed via the BeyoClick™ EdU Cell Proliferation Kit with Alexa Fluor 594 following the manufacturer's instructions (Beyotime, China). In brief, EdU working solution was added to the cells and incubated for 2 h. The cells were treated with fixed and permeabilizing agents, followed by the addiction of a click solution. The samples were subsequently incubated in the dark for 30 min. DAPI was used to stained with nuclei for 3 min. Images were captured via fluorescence microscopy.

Hematoxylin and Eosin (HE) Staining

HE staining was performed via an HE Stain Kit following the manufacturer's instructions (Solarbio, China). In brief, paraffin sections were dewaxed with xylene and dehydrated with alcohol, hematoxylin was used to stain the nuclei, and eosin was used to stain the cytoplasm. After dehydration and sealing with neutral resin, the sections were examined under a microscope, and the images were collected and analyzed.

Masson Staining

Masson staining was performed via a modified Masson trichrome stain kit following the manufacturer's instructions (Solarbio, China). In brief, after the paraffin sections were dewaxed, they were stained with Weigert's iron hematoxylin for 5 min, washed with tap water, and differentiated with 1% hydrochloric acid alcohol for several seconds. The sections were stained with Ponceau red acid fuchsin solution for 5 min and treated with phosphomolybdic acid aqueous solution for approximately 3 min. The sections subsequently were counterstained with aniline blue solution for 5 min and then treated with 1% glacial acetic acid for 1 min. Then, the sections were dehydrated and sealed for microscopic examination, and the images were collected and analyzed.

Wound-Healing Assays

When the cells had reached 80% confluence, they were cultured in serum-free medium. After starvation for 12 h, the medium was discarded, and the cell monolayers were scratched with 200 μL pipette tips. The left and right sides of each intersection, demarcated by the crossing point, were photographed at 0 h and 24 h, respectively.

Immunohistochemical Staining

The sections were incubated in a 60 °C incubator for 60 min, followed by dewaxing and hydration. Antigen retrieval was performed using citrate buffer. The sections were blocked with 5% goat serum and incubated with a-SMA, collagen I and fibronectin antibodies overnight. Secondary antibody incubation and DAB color development were performed. After counterstaining with hematoxylin, the sections were dehydrated, cleared, and sealed. Images were collected on the HAMAMATSU NANO ZOOMER system.

Immunofluorescence

Cells were seeded into climbing pieces, fixed with formaldehyde, and permeabilized with 0.5% Triton X-100. The cells were blocked with BSA blocking solution, incubated with primary antibodies at room temperature for 1 h, and incubated with secondary antibodies in the dark at room temperature for 1 h. A drop of sealing agent was added to the climbing film, and the samples were evaluated under a fluorescence microscope.

MeRIP-m7G-tRNA Sequencing (m7G-tRNA-Seq)

Small RNAs with lengths less than 200 nt were enriched from total RNA with a mirVana Isolation Kit (Thermo Fisher). The GenSeq® M7G MeRIP Kit (GenSeq, Inc.) was used to conduct a MeRIP experiment on the enriched small RNA according to the instructions of the kit. Merip/input RNA samples were demethylated with the alkB enzyme at 37 °C for 100 min. After demethylation, small RNAs were used for small RNA library construction with the GenSeq® Small RNA library prep Kit (GenSeq, Inc). Libraries within the tRNA length range were purified by fragment screening and then sequenced on an Illumina NovaSeq sequencer.

tRNA data were downloaded from the GtRNAdb website. According to their anticodons and scores, representative tRNAs were selected from among these tRNAs. Three bases of CCA were added to the 3' end of the tRNA sequences. After sequencing, image analysis and base recognition, the raw reads were harvested after quality control. First, q30 was used for quality control, and then Cutadapt software (v1.9.3) was used to splice the original reads and remove low-quality reads. Finally, reads with a length ≥15 nt were retained to identify the spliced reads (ie, trimmed reads). The trimmed reads of each sample were subsequently aligned to the preprepared tRNA database via Bowtie2 software (v2.2.4). SAMtools (v1.3.1) was used to count the number of reads that were aligned to each tRNA as the original expression of the tRNA. The results of IP and input were normalized via the TPM method, IP/input was calculated, and the tRNA methylation level was considered to match the normalized results. A fold change >1.5 was considered a significant difference.

tRNA Sequencing (tRNA-Seq)

The tRNA sequencing service was provided by Shanghai Yunxu Biological Company, and the process was performed as follows. Briefly, small RNAs with lengths less than 200 nt were enriched from total RNA with a mirVana Isolation Kit (Thermo Fisher). The enriched small RNAs were treated with alkB enzyme for 100 min at 37 °C. A small RNA library was constructed from the treated samples according to the instructions of the GenSeq® small RNA Library Prep Kit (GenSeq, Inc). Libraries within the tRNA length range were enriched via fragment screening and then sequenced on an Illumina NovaSeq sequencer.

tRNA data were downloaded from the GtRNAdb website. According to the anticodons and scores, representative tRNAs were selected from among these tRNAs. Three bases of CCA were added to the 3' end of each sequence. After Illumina sequencing, image analysis and base recognition, the raw reads were harvested after quality control. First, q30 was used for quality control, and then Cutadapt software (v1.9.3) was used to splice the original reads and remove low-quality reads. Finally, reads with lengths ≥15 nt were retained to identify the spliced reads (ie, trimmed reads). The trimmed reads of each sample were subsequently aligned to the preprepared tRNA database via Bowtie2 software (v2.2.4). SAMtools (v1.3.1) was used to count the number of reads that were aligned to each tRNA as the original expression of the tRNA, and edgeR software was used for data normalization and differential expression screening. Differences were analyzed by t tests. Fold changes >2.0 and p values <0.05 were considered to indicate a significant difference.

mRNA Sequencing (mRNA-Seq)

The ribosomal RNA (rRNA) of the samples was removed via the rRNA Removal Kit (Genseq, Inc)., and the sequencing library was constructed via the GenSeq® Low Input RNA Library Prep Kit (Genseq, Inc.) according to the instructions. Afterward, the constructed sequencing library was subjected to quality control and quantification via a Bioanalyzer 2100 system (Agilent Technologies, USA), followed by 150 bp paired-end sequencing via an Illumina NovaSeq 6000 instrument. After sequencing with the Illumina NovaSeq 6000 sequencer, the original data were obtained. First, the q30 value was used for raw data quality control. We used Cutadapt software (v1.9.3) to remove connectors, low-quality reads, and high-quality clean reads. HISAT2 software was used to align the clean reads to the reference genome, and then HTSeq software (v0.9.1) was used to obtain the original count number. EdgeR was used to normalize and calculate the fold change and p value between the two groups of samples to screen the differentially expressed genes (DEGs), and genes with a fold change >2.0 were considered DEGs. GO function analysis and KEGG pathway analysis were performed on the differentially expressed mRNAs.

Polyribosome-Bound mRNA Sequencing (Ribo-Seq)

Cells were treated with cycloheximide, lysed in lysis buffer and then digested with nuclease. The digested samples were separated into single ribosomes with a size exclusion column. Fragment selection was performed on RNA fragments that were protected by ribosomes via polyacrylamide gel electrophoresis, after which rRNA was removed from the samples via rRNA removal reagents. After purification, the RNA ends were repaired, and a 3 'connector was added; then, the samples were transformed into cDNA through reverse transcription. cDNA was purified via polyacrylamide gel electrophoresis, cyclized, and amplified via PCR. The amplified library that was obtained was purified and sequenced on a NovaSeq

sequencer (Illumina). After sequencing with an Illumina NovaSeq 6000 sequencer, the raw data were obtained. First, the Q30 value was used for raw data quality control. Cutadapt software (v1.9.3) was used to remove connectors, low-quality reads, and high-quality clean reads. Bowtie was used to compare the disconnected data to rRNA sequences and to obtain clean reads that had not been aligned to rRNA. Tophat2 software was used to compare the clean reads to the reference genome. Then, HTSeq software (v0.9.1) was used to obtain the original count number, edgeR or DESeq2 was used for standardization, and the multiple changes and p values between the two groups of samples were calculated to identify DEGs. By default, edgeR was used for differential analysis. Correlation analysis between the mRNA-seq and Ribo-seq data was performed. The ratio of the FPKM value of each gene in Ribo-seq to the FPKM value in mRNA-seq was considered the translation efficiency (TE). A fold change >2.0 was considered a meaningful difference.

Northern Blotting and Northwestern Blotting

For northern blotting, 2 μg total RNA samples was mixed with RNA loading buffer (2X) and denatured at 65 °C for 15 min. Then, the samples were subjected to 15% urea-PAGE in 1X TBE buffer. The separated RNAs were then transferred to a positively charged nylon membrane, and cross-linking was performed via ultraviolet (UV) light. The tRNAs or U6 snoRNAs were blotted with the corresponding digoxigenin-labeled probes. For Northwestern blotting, the RNA-containing nylon membranes were crosslinked with UV light and blotted with an anti-m7G antibody (RN017M; Medical Biological Laboratories, Nagoya, Japan). After incubation of BeyoECL Moon buffer with a nylon membrane, the signals were detected according to previous reports.[16–18]

Coomassie Blue Staining

The PAGE gel was soaked in BeyoBlue™ Coomassie Blue Super Fast Staining Solution (Beyotime Biotechnology, China) and dyed at room temperature on a sway shaker for 30 min. Then, the decolorization solution was discarded, and deionized water was added for decolorization on a shaker.

Coimmunoprecipitation (CoIP)

The cells were lysed and incubated with the indicated antibodies overnight. Then, protein A/G-MagBeads were added to the sample, and elution was conducted with elution buffer.

Seahorse Assay

The extracellular acidification rate (ECAR) of the cells was measured via a Seahorse XF96 Flux Analyzer (Seahorse Bioscience, Agilent). In brief, 1×10^4 cells were seeded into Agilent Seahorse XFe96 plates and cultured for 12 h in a standard incubator. Afterward, the cells were treated with 10 mM glucose, 2 μM oligomycin or 2-deoxy-D-glucose at different ports of the Seahorse cartridge.

Statistical Analysis

All the continuous variables are presented as the means ± standard deviations. Differences between three groups were analyzed by one-factor ANOVA. The data were analyzed and visualized via SPSS 21.0 software (SPSS, Chicago, IL, USA) and GraphPad Prism 7 (GraphPad, San Diego, CA, USA). $P< 0.05$ was considered to indicate statistically significant differences.

Results

RA Prevented RIPF and Inhibited the Progression of FMT

Our prior study revealed that RA can alleviate RIPF in rats,[9] and FMT plays a core role in the pathogenesis of organ fibrosis.[19] In the present study, we further evaluated the effects of RA on RIPF and FMT in C57BL/6 mice. RA-treated mice had improved lung morphology, with less lung collapse and fewer fibrous nodules (Figure 1A). The lung index, which reflects the ratio of lung/body weight, was significantly lower in the RA+IR group than in the IR group (Figure 1B). Compared with irradiated mice that did not receive RA treatment, RA-treated mice exhibited attenuated

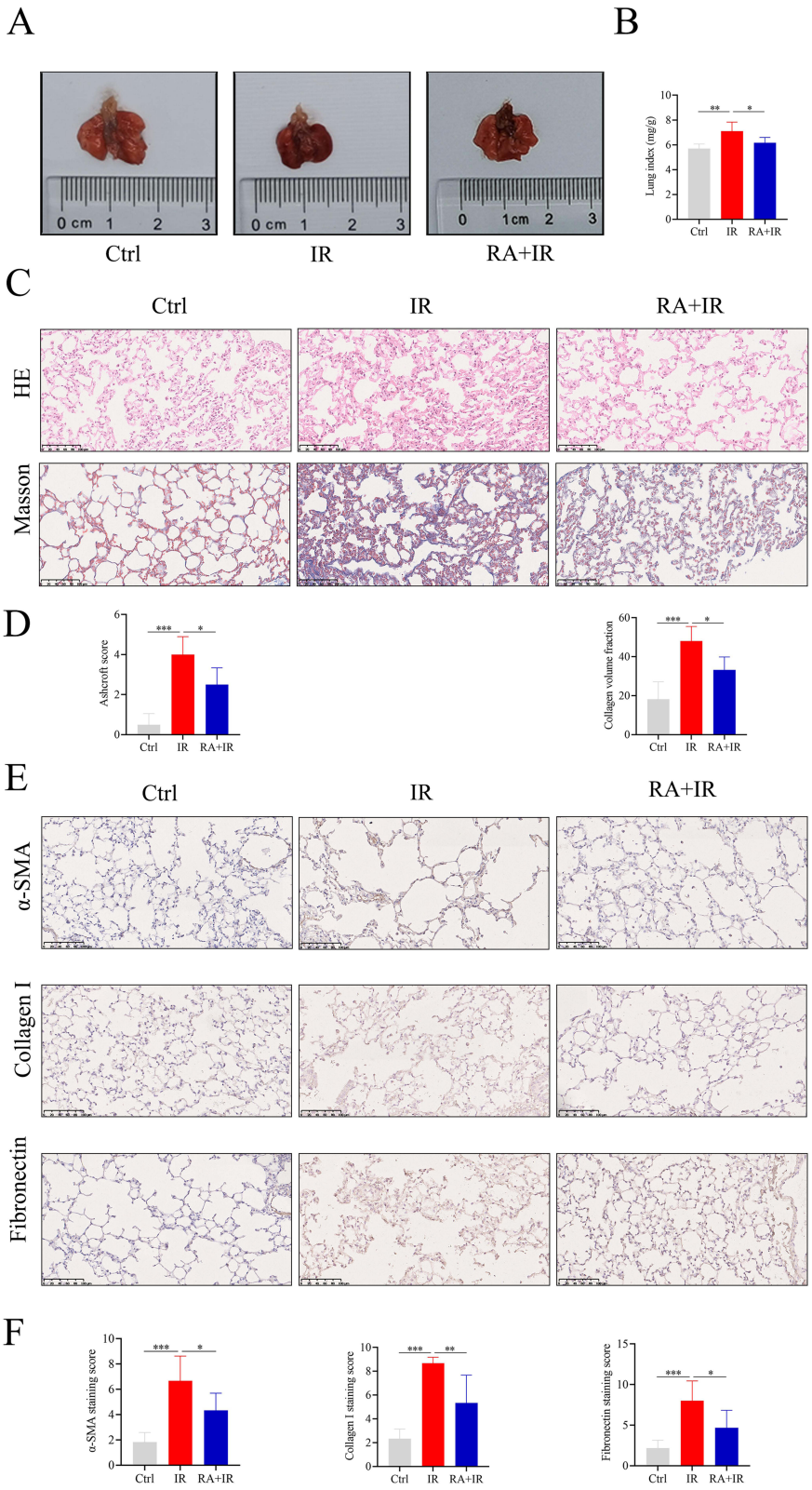

Figure 1 Effects of RA on pathological changes and collagen deposition in the lung tissue of mice at 24 weeks after total thoracic irradiation. (**A**) Representative images of lung tissues. (**B**) The lung index, which refers to the lung/body weight ratio, is shown. (**C**–**F**) Representative images and statistical analysis of hematoxylin–eosin staining, masson staining and immunohistochemical staining of FMT markers. Scale bars, 100 μm. The precise n value (number of biologically independent replicates) is 6. *P < 0.05, **P < 0.01, ***P < 0.001.

fibrosis, as indicated by a reduction of thickened alveolar walls, fewer fibrotic foci and less collagen deposition, which was in line with decreases in the ashcroft score and collagen volume fraction (Figure 1C and D). The expression of the FMT markers α-SMA, collagen I and fibronectin in RA-treated mice was lower than that in irradiated mice (Figure 1E and F). These results indicated that RA exerted an antifibrotic effect on the lung tissues of RIPF model mice and suppressed the progression of FMT in irradiated mouse lung tissues.

RA Decelerated the Progression of FMT Through the Exosome Pathway

To explore the mechanism underlying RIPF, exosomes derived from lung epithelial cells were identified and quantified via transmission electron microscopy. Nanoparticle tracking analysis revealed that the average sizes of the exosomes isolated from the TC-1 and MLE-12 cells were approximately 84.49 and 86.93 nm, respectively (Figure 2A and B and Supplementary Figure 1A and B). Additionally, the uptake of exosomes by MLFs was observed after 24 h of coincubation with TC-1 cell-derived exosomes (TC-1-exos) or MLE-12 cell-derived exosomes (MLE-12-exos) labeled with PKH67 (red) (Figure 2C and Supplementary Figure 1C). Interestingly, immunofluorescence staining revealed that incubating MLFs with exosomes derived from irradiated epithelial cells with RA intervention (RA+IR-TC-1/MLE-12-exos) inhibited the induction of α-SMA expression in the MLFs (Figure 2D and Supplementary Figure 1D). In addition, EdU staining and wound-healing assays revealed that treating MLFs with RA+IR-TC-1/MLE-12-exos significantly decreased the ability of IR-TC-1/MLE-12-exos to induce proliferation and migration (Figure 2E and F and Supplementary Figure 1E and F). Together, these results indicated that RA suppressed FMT of MLFs induced by exosomes derived from irradiated lung epithelial cells.

RA Reversed the Increase in the Expression and m7G Modification Level of tRNAs Induced by Irradiation in Lung Epithelial Cells

Many studies have demonstrated that tRNA epigenetic modifications are associated with the pathological processes of numerous diseases, including organ fibrosis.[18,20–22] To assess the correlation between RIPF and tRNA m7G modification, which is one of the most common epigenetic modifications, we conducted m7G-tRNA-seq and tRNA-seq analyses were performed in TC-1 cells (Supplementary Tables 1 and 2). We found that the expression and m7G modification levels of tRNA-ArgCCG and tRNA-CysGCA were significantly greater in the IR group than in the Ctrl group (Figure 3A and B). Northwestern and northern blotting analyses further confirmed these results and revealed that the increase in the expression and m7G modification level of tRNA-ArgCCG and tRNA-CysGCA caused by irradiation could be reversed by RA (Figure 3C and D). We then investigated the effect of RA on the METTL1/WDR4 complex, which is the main catalytic complex for tRNA m7G modification in eukaryotic cells. The Western blotting results revealed that RA reduced the upregulation of METTL1 and WDR4 protein expression induced by irradiation (Figure 3E). In addition, silencing METTL1 and WDR4 eliminated the promoting effect of irradiation on the expression and m7G modification of the indicated tRNA (Figure 3F and G). Taken together, our results indicated that tRNA levels and m7G modifications increased in lung epithelial cells after irradiation and that RA reversed these changes.

RA Suppressed the Process of FMT by Downregulating METTL1/WDR4-Mediated tRNA m7G Modifications in the Exosomes of Lung Epithelial Cells

To further verify if there is an increase in tRNA levels and m7G modifications in exosomes, we performed Northwestern blotting, northern blotting and immunofluorescence staining. The results revealed that the levels of m7G modification and tRNA expression in the exosomes of irradiated lung epithelial cells were greater than those in the control cells, while RA treatment partially reversed the effects of irradiation on the exosomes of lung epithelial cells (Figure 4A). In addition, exosomes derived from TC-1 cells overexpressing METTL1/WDR4 (oeMETTL1/MDR4-TC-1-exo) exhibited elevated tRNA expression and m7G modification levels, while no similar results were observed in the RA intervention group (Figure 4B). The m7G modification levels in MLFs incubated with exosomes from TC-1 cells in the Ctrl, IR, and RA+IR groups (Ctrl-TC-1-exo, IR-TC-1-exo and RA+IR-TC-1-exo) were analyzed via northwestern and northern blotting. Our results confirmed that an upregulation of tRNA m7G modifications in both the IR-TC-1-exo group and RA+IR-TC-1-exo

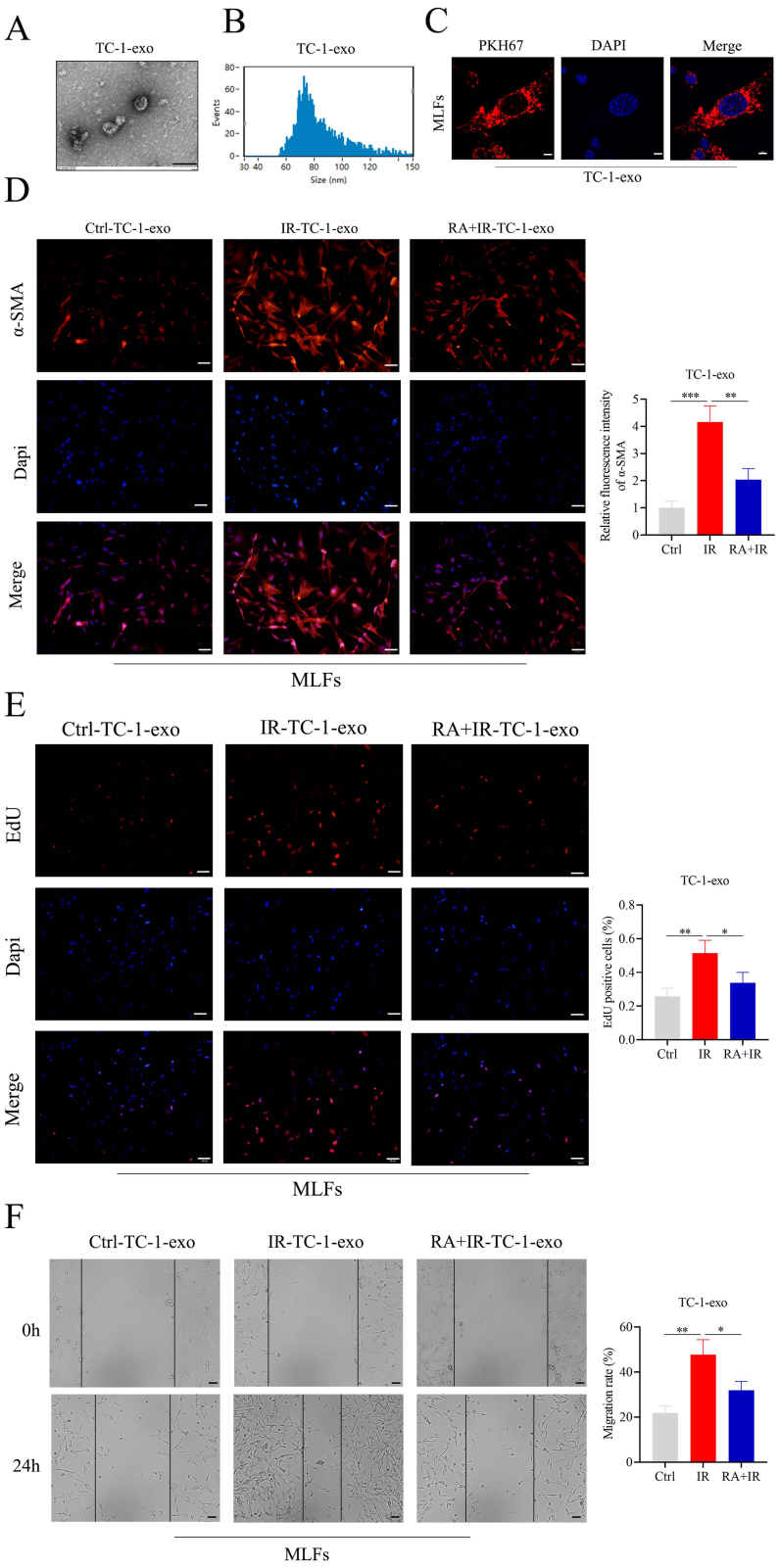

Figure 2 RA decelerated the progression of FMT in MLFs through the exosome pathway in TC-1 cells. (**A**) Exosomes derived from TC-1 cells were characterized via electron microscopy. Scale bars, 100 nm. (**B**) Distribution of the size and concentration of the extracted exosomes. (**C**) PKH67-labeled exosomes derived from TC-1 cells were ingested by MLFs. Scale bars, 10 μm. (**D**) The expression levels and statistical analysis of α-SMA were detected by immunofluorescence staining. Scale bars, 50 μm. (**E**) Cell viability was tested by EdU staining. Scale bars, 50 μm. (**F**) Migration ability was detected by a wound healing assay. Scale bars, 50 μm. The precise n value (number of biologically independent replicates) is 3. *P < 0.05, **P < 0.01, ***P < 0.001.

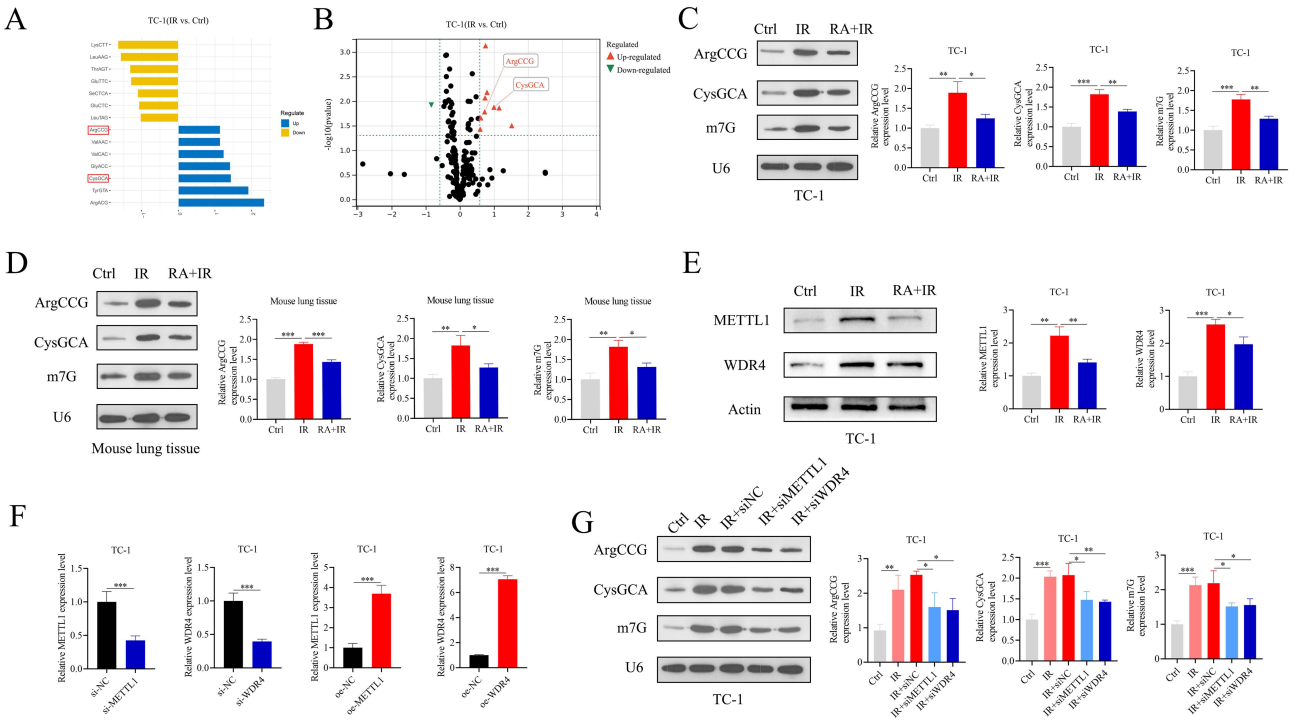

Figure 3 RA reversed the increase in tRNA expression and m7G modification levels in irradiated lung epithelial cells. (**A**) Quantification of the m7G modification level of tRNAs. (**B**) Expression profile of tRNAs. Fold Change cut-off: 1.5, P-value cut-off: 0.05. (**C** and **D**) Northwestern and northern blotting of the indicated tRNAs was performed in TC-1 cells and mouse lung tissue. (**E**) The expression levels of the METTL1/WDR4 complex were evaluated via Western blotting. (**F**) The efficiency of both knockdown and overexpression of METTL1 and WDR4 genes were confirmed by qRT–PCR. (**G**) The effects of METTL1 and WDR4 on tRNA expression and m7G modification were detected via northwestern and northern blotting. The precise n value (number of biologically independent replicates) is 3. *P < 0.05, **P < 0.01, ***P < 0.001.

group, with a particularly greater increase observed in the former (Figure 4C). In addition, immunofluorescence staining revealed that incubating MLFs with oeMETTL1/MDR4-TC-1/MLE-12-exo plus RA diminished the expression of α-SMA induced by these exosomes (Figure 5A and Supplementary Figure 2A). Consistently, EdU staining and wound-healing assays indicated that MLFs treated with oeMETTL1/MDR4-TC-1-exos and RA had reduced proliferation and migration abilities than those not treated with RA (Figure 5B and C and Supplementary Figure 2B and C). In conclusion, these results confirmed that RA had a negative regulatory effect on the m7G modification level of tRNAs in the exosomes of lung epithelial cells.

RA Regulated the Translation Efficiency of SPHK1 and Subsequently Affected the Interaction Between SPHK1 and NAT10

Since tRNA is involved mainly in protein synthesis, abnormal tRNA expression may affect mRNA translation. In our present study, Ribo-seq and mRNA-seq analyses were performed to explore the underlying target mRNAs. We identified mRNAs whose expression levels did not significantly differ according to mRNA-seq but whose translation efficiency significantly differed according to Ribo-seq as target genes for tRNA modification. Compared with the MLFs in the Ctrl-TC-1-exo group, the MLFs in the IR-TC-1-exo group presented 3101 mRNAs with decreased translation ratios (TRs) and 2086 mRNAs with increased TRs (Supplementary Table 3), among which SPHK1 had a significantly increased TR (Figure 6A). SPHK1 has been reported to regulate pulmonary, hepatic, and renal fibrosis,[23–25] yet the role of SPHK1 in RIPF has not been elucidated. KEGG enrichment analysis of these mRNAs with increased TRs revealed significant enrichment in the Wnt signaling pathway, MAPK signaling pathway, and ECM-receptor interaction (Figure 6B). qRT–PCR and Western blotting further revealed that IR-TC-1-exos and RA+IR-TC-1-exos had little effect on the mRNA expression of SPHK1 in MLFs but had a significant effect on protein expression (Figure 6C and D). The results of the polyribosome-qPCR assay confirmed that the translation efficiency of SPHK1 in the IR-TC-1-exo group was greater than that in the Ctrl-TC-1-exo group, whereas the

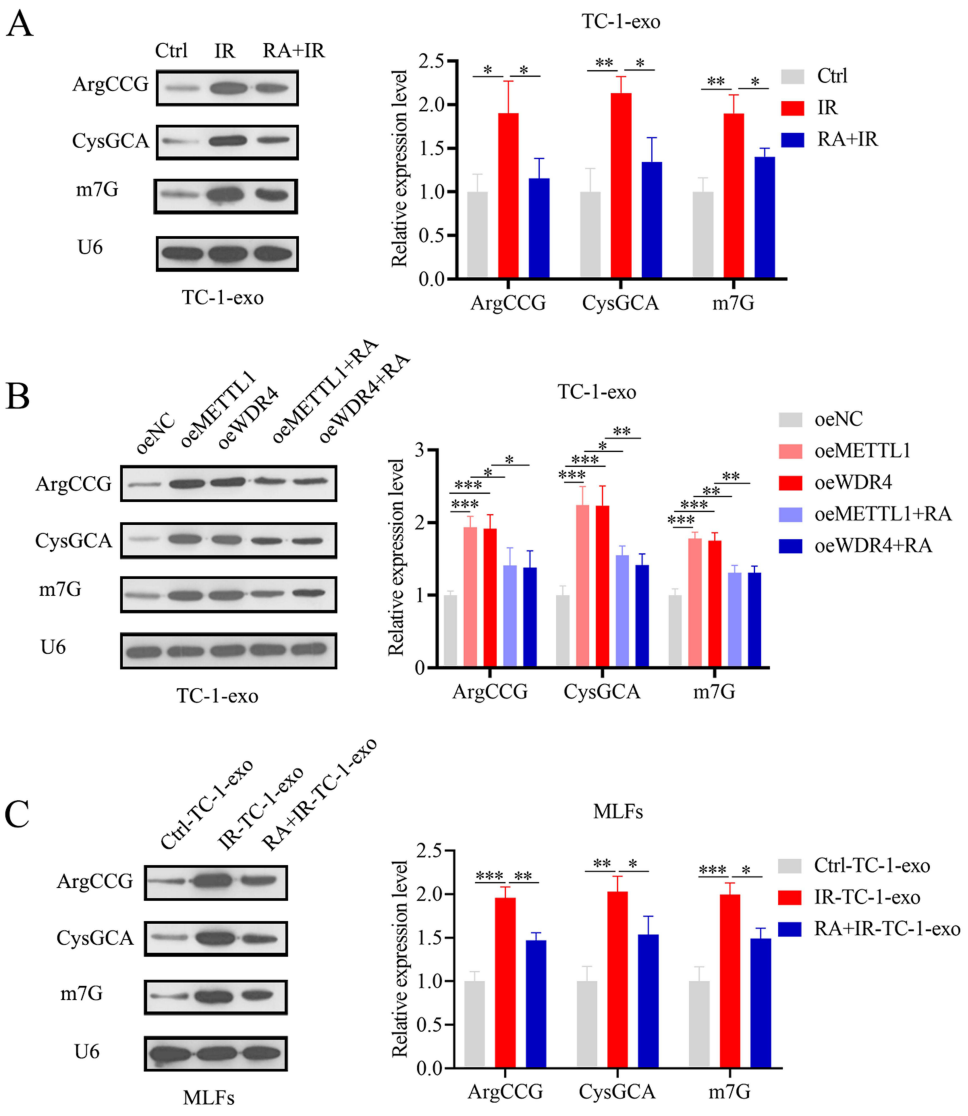

Figure 4 RA affected the METTL1/WDR4-mediated tRNA m7G modification of MLFs via exosomes. (**A** and **B**) Expression levels of representative m7G-modified tRNAs in exosomes were examined by northwestern and northern blotting using the indicated tRNA probes. (**C**) MLFs were incubated with exosomes derived from TC-1 cells, and the expression and m7G modification levels of the indicated tRNAs were detected via northwestern and northern blot assays. The precise n value (number of biologically independent replicates) is 3. *P < 0.05, **P < 0.01, ***P < 0.001.

translation efficiency of SPHK1 was lower in the RA+IR-TC-1-exo group than in the IR-TC-1-exo group (Figure 6E). Recently, NAT10 was reported to enhance pulmonary fibrosis.[26] On the basis of HDOCK database retrieval, NAT10 was found to potentially bind to SPHK1 (Figure 6F). Coomassie blue staining further suggested the potential interaction between NAT10 and SPHK1 (Figure 6G). Moreover, CoIP assays verified that SPHK1 directly interacted with NAT10 (Figure 6H). Taken together, our results indicate that IR-TC-1-exos increased the translation ratio of SPHK1 in MLFs and affected the binding between the SPHK1 and NAT10 proteins, whereas RA can counteract the effects of IR-TC-1-exos on MLFs.

RA Diminished Glycolysis by Reducing Acetylated PFKFB3 and Cytoplasmic Translocation

Myofibroblasts may use aerobic glycolysis as an additional source of bioenergetics and biosynthesis to meet the demands related to rapid growth and proliferation.[27] In this study, compared with that of the control group, the ECAR of the IR-TC -1-exo group was significantly greater, whereas that of the RA+IR-TC-1-exo group was only slightly greater (Figure 7A), indicating that RA may inhibit the glycolysis of MLFs via the exosome pathway derived from lung epithelial cells.

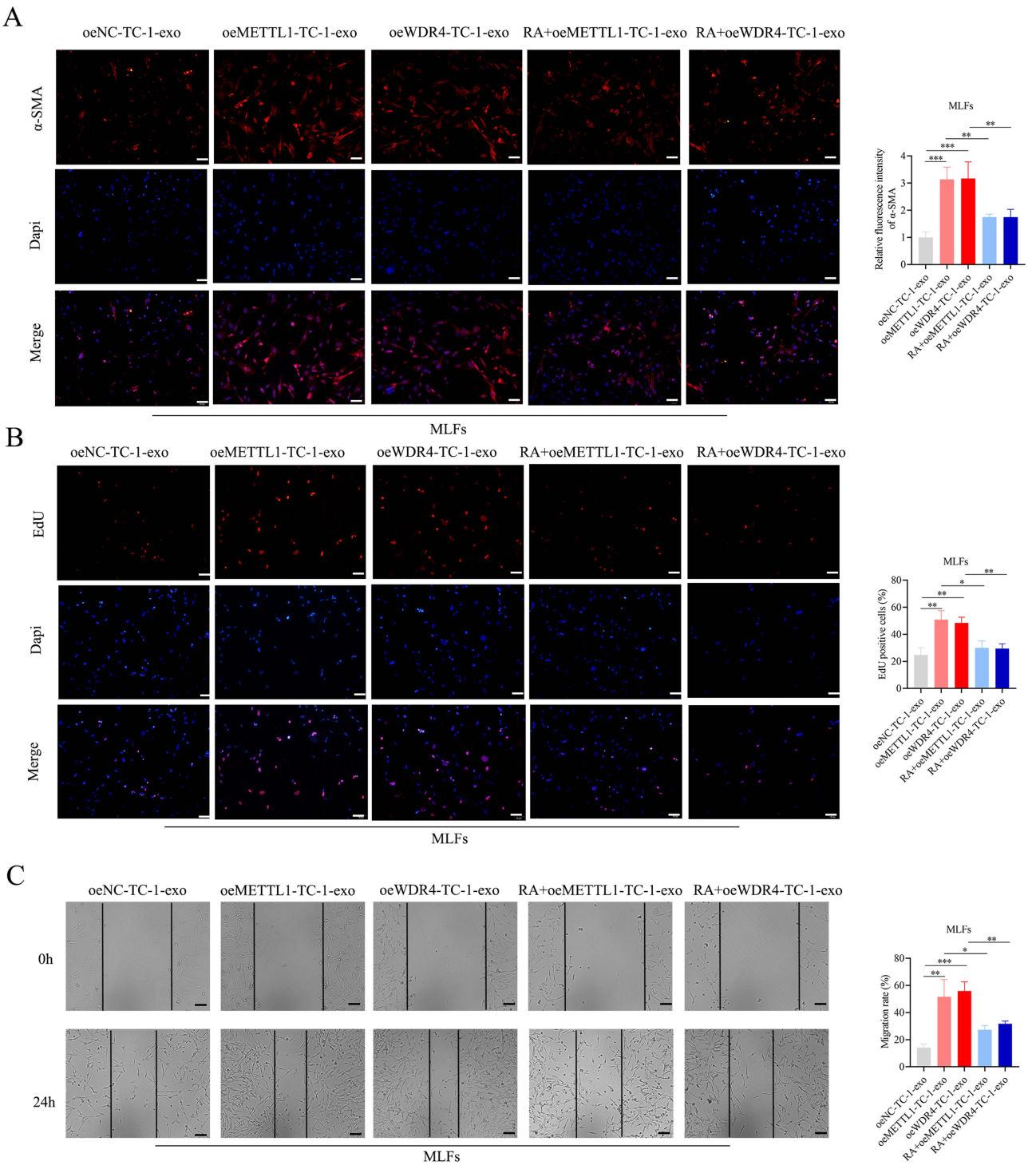

Figure 5 RA suppressed the process of FMT in MLFs by downregulating METTL1/WDR4-mediated tRNA m7G modification via exosomes of TC-1 cells. (**A**) The expression of α-SMA was assessed via immunofluorescence staining. Scale bars, 50 μm. (**B**) Cell viability was tested via EdU staining. Scale bars, 50 μm. (**C**) Migration ability was detected by a wound healing assay. Scale bars, 50 μm. The precise n value (number of biologically independent replicates) is 3. *P < 0.05, **P < 0.01, ***P < 0.001.

Previous studies have shown that the acetylation of metabolic enzymes is a critical mechanism underlying metabolic modulation.[28] PFKFB3, a key enzyme in glycolysis, has been proven to be a driving factor for various organ fibrosis diseases,[29–31] which prompted us to investigate the mechanism underlying the regulation of PFKFB3 by exosomes. The results showed that IR-TC-1-exo treatment increased the acetylation level of PFKFB3 and that the addition of RA

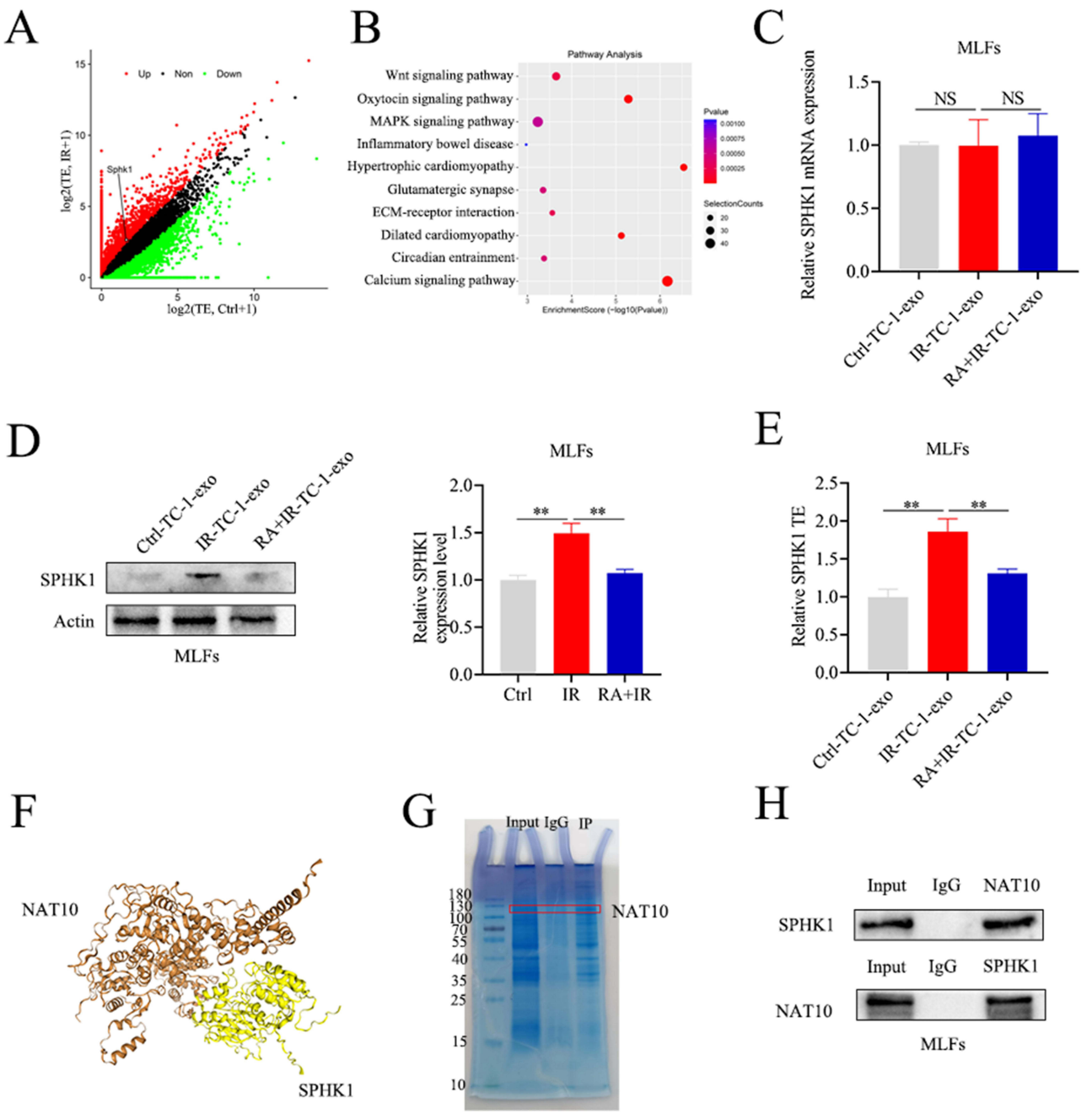

Figure 6 SPHK1 is a target gene of m7G-modified tRNA and interacts with NAT10. (**A**) Ribo-seq and mRNA-seq analyses were performed to explore the target mRNAs. (**B**) KEGG analysis of increased translated mRNAs. (**C** and **D**) qRT–PCR and Western blot analysis of SPHK1 in MLFs. (**E**) qRT–PCR-based TE analysis of SPHK1 was performed with polyribosome mRNAs. (**F**) The relationship between SPHK1 and NAT10 was predicted via the HDOCK database. (**G**) SPHK1-interacting proteins were identified via Coomassie blue staining. (**H**) The interaction of the SPHK1 protein with the NAT10 protein was evaluated via CoIP. The precise n value (number of biologically independent replicates) is 3. **P < 0.01.

partially counteracted this effect (Figure 7B). NAT10 belongs to the Gcn5-related N-acetyltransferase family, which has been reported to acetylate RNAs and proteins.[32] Interestingly, we observed that Remodelin (an inhibitor of NAT10) reduced the acetylation of PFKFB3 (Figure 7C). PFKFB3 is localized to the nucleus, possibly because of the inclusion of a classical nuclear localization signal (KKPR, amino acids 472–475).[33] Mass spectrometric analysis by Li et al revealed six lysine (K) residues in PFKFB3 that undergo acetylation (K12, K284, K302, K451, K472 and K473).[33] Consequently, we speculated that K472 and K473 were the major acetylation sites that interfered with the nuclear localization of PFKFB3. As expected, we found that mutation of the K472R and K473R sites greatly reduced the acetylation of

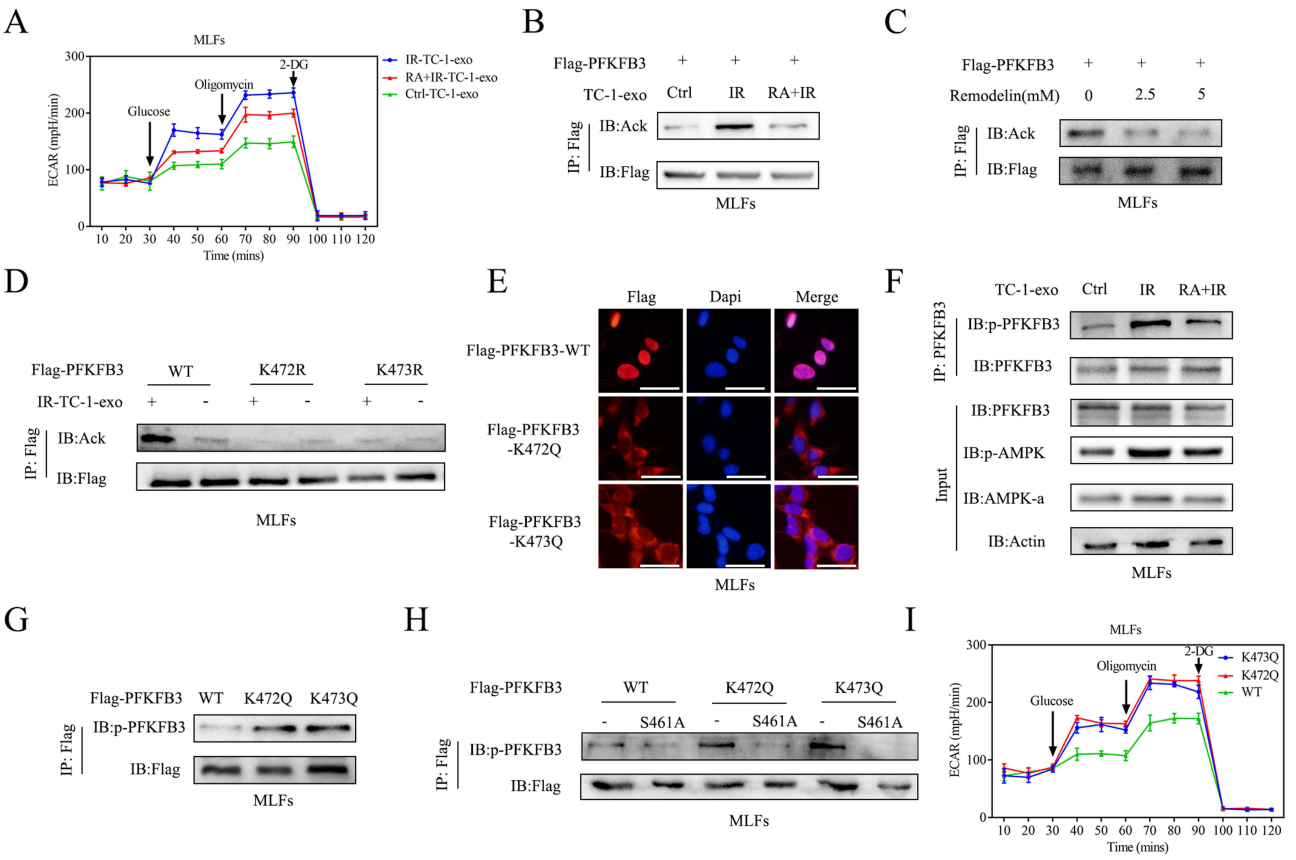

Figure 7 RA diminished glycolysis by reducing acetylated PFKFB3 and cytoplasmic translocation. (**A**) ECARs were evaluated via a Seahorse XFe96 Extracellular Flux Analyzer. (**B**) The acetylation levels of PFKFB3 were examined via Western blotting. (**C**) After treatment with Remodelin (an inhibitor of NAT10), the acetylation levels of PFKFB3 in MLFs were examined. (**D**) The acetylation sites of PFKFB3 were examined by immunoprecipitation. (**E**) The effects of the K472Q and K473Q mutations on the distribution of PFKFB3 in MLFs were assessed via immunofluorescence staining. Scale bars, 50 μm. (**F**) Phosphorylation levels of PFKFB3 and AMPK were examined. (**G** and **H**) The effects of the K472Q and K473Q mutations on the phosphorylation levels of PFKFB3 were examined. (**I**) The effects of the K472Q and K473Q mutations on the ECAR were evaluated via the Seahorse assay.

PFKFB3 (Figure 7D). FISH assays revealed that wild-type (WT) PFKFB3 was localized in the nucleus, whereas the K472Q and K473Q mutants were localized in the cytoplasm (Figure 7E). In addition, cytoplasmic PFKFB3 has a stronger effect on promoting glycolysis.[34] AMPK activates PFKFB3 and promotes glycolysis through the phosphorylation of PFKFB3 at S461.[35] To verify that the cytoplasmic localization of PFKFB3 affects its phosphorylation at the S461 site, Western blotting was performed. S461 phosphorylation was increased in the IR-TC-1-exo group, and this effect was reversed in the RA+IR-TC-1-exo group (Figure 7F). Compared with cells expressing WT PFKFB3, cells expressing the K472Q or K473Q mutant presented greater phosphorylation of S461 and activity of PFKFB3 (Figure 7G and H) as well as a greater ECAR (Figure 7I). In addition, an IHC experiment was conducted to scrutinize the expression of SPHK1 and pPFKFB3 in the lung tissue of the Ctrl, IR, and RA+IR groups. The results revealed that irradiation led to an upregulation in the expression of both SPHK1 and pPFKFB3. Interestingly, the administration of RA mitigated this IR-induced increase in the expression of both SPHK1 and pPFKFB3, indicating its potential regulatory effect (Figure 8).

Taken together, these results indicated that IR-TC-1-exos promoted PFKFB3 acetylation at K472 and K473 and induced the translocation of PFKFB3 from the nucleus to the cytoplasm in MLFs. Additionally, cytoplasmic PFKFB3 was phosphorylated by AMPK, and the glycolytic process was thereby enhanced. On the other hand, RA reduced these changes (Figure 9).

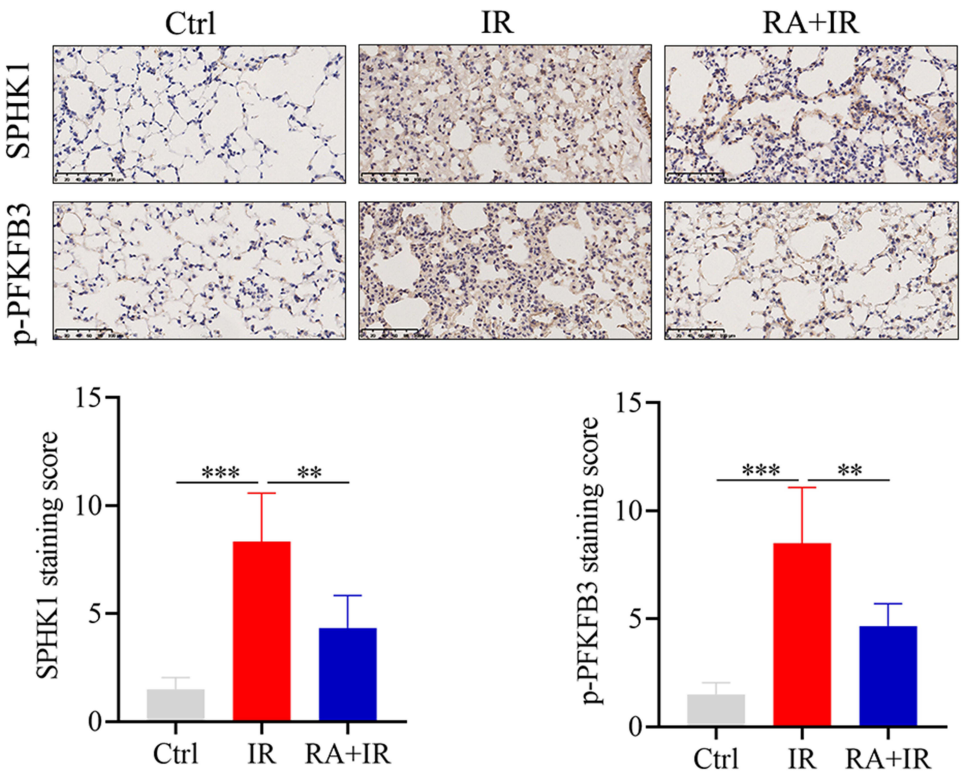

Figure 8 RA counteracted the upregulated expression of SPHK1 and pPFKFB3 that is provoked by IR. Immunohistochemical investigation of SPHK1 and pPFKFB3 expression in mouse lung tissues from the Ctrl, IR and RA+IR groups. Scale bars, 100 μm. The precise n value (number of biologically independent replicates) is 3. **P < 0.01, ***P < 0.001.

Discussion

RIPF is a serious complication of radiotherapy that is difficult to reverse. At present, there is a lack of effective treatment methods. In this study, we present several intriguing findings: high-throughput sequencing results revealed a significant increase in both the expression and m7G modification level of tRNAs within exosomes derived from irradiated lung epithelial cells. In addition, RA inhibited the translation efficiency and protein expression of SPHK1, which is regulated by tRNA m7G modification, and suppressed the acetylation of PFKFB3 in the nucleus. Moreover, RA decreased the level of phosphorylated PFKFB3 in the cytoplasm and ultimately reduced FMT triggered by glycolysis in lung fibroblasts.

Numerous studies have shown that cells can transmit important signaling molecules, such as RNA and proteins, and thus promote FMT through exosomes. Huang et al reported that exosomal SPP1 derived from silica-treated macrophages can trigger FMT and promote pulmonary fibrosis to form silicosis.[36] Li et al reported that miR-192-5p in exosomes derived from adipose tissue mesenchymal stem cells reduced collagen deposition and FMT by targeting the IL-17RA/Smad signaling axis, thereby exerting an inhibitory effect on scar hyperplasia.[37] In this study, we extracted exosomes from irradiated lung epithelial cells. Transmission electron microscopy and nanoparticle tracing analysis confirmed that irradiated TC-1 cell-derived exosomes can be taken up by MLFs, which promotes the expression of the FMT marker protein α-SMA and enhances the proliferation and migration of MLFs. Compared with those from IR-TC-1-exos, exosomes from irradiated lung epithelial cells significantly inhibited the FMT of MLFs. These results indicate that RA can inhibit FMT via exosomes derived from lung epithelial cells.

In recent years, mounting evidence has shown that epigenetic modifications of tRNAs are associated with the pathological processes of various diseases. For example, dysregulated tRNA m7G modification has a carcinogenic effect on esophageal squamous cell carcinoma.[18] The presence of NSUN2 gene mutations in patients resulted in a deficiency of specific 5-cytosine methylation at the C47 and C48 sites of tRNAAsp, leading to significant intellectual impairment, facial abnormalities, and distal myopathy.[20] Another study has reported that the key pathogenesis caused by CDKAL1

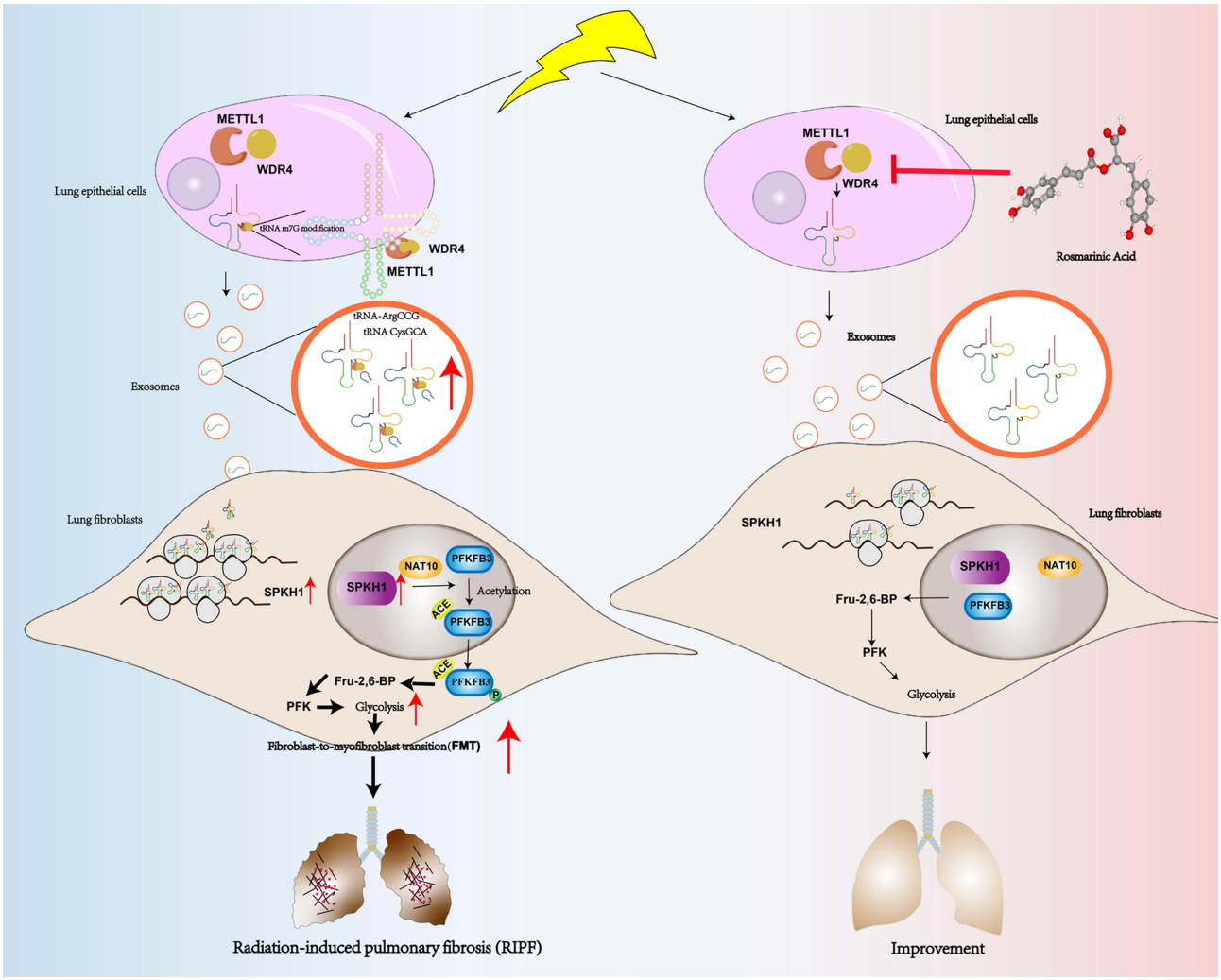

Figure 9 Schematic model of RA protection against RIPF.

deficiency in diabetes patients is β-mistranslation of Lys codons in cells, which leads to a decrease in glucose-stimulated insulin synthesis; the underlying molecular mechanism may be related to the 2-methylthio-modification of N6-threonyl carbonyladenosine at position 37 in $tRNA_{UUUU}^{Lys3}$.[21] However, there is currently no research on the epigenetic modification of tRNA in RIPF.

m7G modification is one of the most common epigenetic modifications of RNA and plays an important role in maintaining the integrity and stability of tRNA. Our study conducted m7G-tRNA-seq and tRNA-seq analyses and revealed that m7G modification and the expression of tRNA-ArgCCG and tRNA-CysGCA were most substantially increased in irradiated lung epithelial cells. Further validation revealed that RA treatment reversed these changes and radiation-induced high expression of m7G methyltransferase complex components (METTL1 and WDR4). We also found that after METTL1 and WDR4 were upregulated in lung epithelial cells and MLFs were incubated with their exosomes, the expression level of α-SMA significantly increased, and the proliferation and migration of the MLFs increased. These results suggested that RA may downregulate the transmission of tRNA-ArgCCG and tRNA-CysGCA to MLFs by inhibiting these tRNA m7G modifications in lung epithelial cells, ultimately slowing the FMT process in MLFs.

To further investigate the protein translation dysregulation caused by abnormal tRNA m7G modification, we conducted Ribo-seq and mRNA-seq analyses. Among the 2086 mRNAs that displayed a notable augmentation in TRs, SPHK1 exhibited a remarkably enhanced TR. SPHK1, a crucial kinase, plays a pivotal role in regulating the metabolism of damaged tissues and modulates the progression of pulmonary fibrosis. Notably, Bleomycin has been reported to

exacerbate fibrosis by activating the pulmonary SPHK1/S1P pathway and its downstream Hippo target yap/taz profibrotic genes.[38] Additionally, genetic and pharmacological inhibition of SPHK1 has been shown to mitigate bleomycin-induced pulmonary fibrosis in mice.[39] Through Ribo-seq and mRNA-seq analyses, SPHK1 was found as an essential downstream target gene for tRNA modification. While its expression levels remained largely unchanged based on mRNA-seq analysis, its translation efficiency was significantly altered as indicated by Ribo-seq data. Our research further illuminated that IR-exos remarkably enhanced the expression of the SPHK1 protein, while exhibiting negligible effects at the mRNA level. Furthermore, the polysome qPCR results indicated an increase in the translation efficiency of SPHK1 in MLFs treated with IR-exo, these results revealed SPHK1 protein is regulated by tRNA m7G modification. Following the detection of elevated SPHK1 level, bioinformatic prediction and subsequent CoIP assays uncovered a significant interaction between SPHK1 and NAT10. NAT10, an acetyltransferase, contributes to various cellular biological processes by acetylating RNA and other molecules. Recent studies have also highlighted NAT10's role in maintaining cellular homeostasis under stressful conditions, achieved through the acetylation of critical checkpoint proteins such as p53, PARP1, and MORC2.[40]

Subsequently, we explored the downstream molecules regulated by NAT10. Glycolysis is an important metabolic pathway that occurs in almost all living cells. Research has shown that glycolysis is increased in fibroblasts and myofibroblasts of the liver, lungs, and kidneys during chronic inflammation and fibrosis.[41] In addition, during the process of fibrosis in organs such as the lungs, cell-dependent energy metabolism gradually shifts from oxidative phosphorylation to glycolysis, which is also known referred to as the Warburg effect.[42] However, the role of glycolysis in RIPF is not yet clear. PFKFB3 catalyzes the synthesis and hydrolysis of the small molecule fructose-2,6-diphosphate, which is a potent activator of the glycolytic pathway. Among the four members of the PFKFB protein family, PFKFB3 is the only protein that is located in the nucleus.[43] We wondered whether NAT10 would act on PFKFB3. The subsequent CoIP assay and cytological function experiments suggested that NAT10 promotes the acetylation of PFKFB3, which in turn leads to increased glycolysis. Our study revealed that after MLFs were incubated with IR-TC-1-exos, the level of acetylated PFKFB3 at the K472 and K473 sites was increased, as did the level of phosphorylation at the S461. On the other hand, RA inhibited these changes. FISH experiments revealed that the PFKFB3 protein was originally expressed in the nucleus of MLFs, whereas the PFKFB3 protein was translocated from the nucleus to the cytoplasm after incubation with IR-TC-1-exos in MLFs. However, treatment with RA reversed the nuclear–cytoplasmic translocation of PFKFB3. Similar results were also described by Li et al, who reported that the chemotherapy drug cisplatin accumulated PFKFB3 in the cytoplasm and promoted glycolysis.[33] Specifically, the lysine residue at position 472 of the PFKFB3 protein was acetylated, which inactivated the nuclear localization signal of PFKFB3 and promoted its retention in the cytoplasm. PFKFB3, which is located in the cytoplasm, is more susceptible to phosphorylation by the kinase AMPK, leading to the activation of PFKFB3 and promoting glycolysis, thereby protecting cells from apoptosis. Together, our findings reveal a novel mechanism for regulating the activity of the metabolic regulatory enzyme PFKFB3 through acetylation in RIPF and suggest that targeted inhibition of PFKFB3 by RA may be a new clinical strategy for treating RIPF.

In the correlation studies between RA and lung diseases, a significant portion of research has concentrated on fibroblasts and lung epithelial cells. For instance, RA has been observed to mitigate the detrimental effects of anoxia/reoxygenation on the human lung epithelial cell line A549, encountered in pulmonary ischemia/reperfusion injury.[44] Furthermore, it has been documented to alleviate the proliferation of the human embryonic lung fibroblasts cell line IMR-90, thereby inhibiting RIPF.[9] Additionally, RA has been found to retard pulmonary fibrosis by downregulating the phosphorylation of the TGF-β1/Smad and MAPK signaling pathways in TGF-β1-induced mouse fibroblast L929 cells.[45] There is some study highlighting the effects of RA on alveolar type II cells, demonstrating a 40% reduction in cell viability with RA treatment.[46] However, there are relatively few reports exploring the impact of RA on cellular interactions. Our research is the first to report the influence of RA on fibroblasts through exosomes released by lung epithelial cells, albeit at a preliminary stage. This study is subject to several limitations that merit further attention. Firstly, we are unable to fully discount the potential impact of RA on other diverse cellular types. Secondly, our choice to exclusively employ male mice as subjects stems from the scientific literature[47–49] that have successfully established pulmonary fibrosis models in this gender, yet this may limit the study's generalizability. Lastly, the question of whether RA exerts its effects on other cell types in the lung remains an unexplored terrain.

Conclusion

In summary, the findings presented here suggested that RA alleviated RIPF by downregulating tRNA m7G modification and that expression level regulated FMT through the exosome pathway. RA may be a potential therapeutic drug for slowing the progression of RIPF.

Abbreviations

CoIP, Coimmunoprecipitation; Ctrl, Control; Ctrl-TC-1-exo, Exosomes of normal TC-1 cells; ECAR, Extracellular acidification rate; FMT, Fibroblast to myofibroblast transition; HE, Hematoxylin-Eosin; IR, Irradiation; IR-TC-1-exo, Exosomes of the irradiated TC-1 cells; m7G, N7-methylguanosine; m7G-tRNA-seq, MeRIP-m7G-tRNA sequencing; MLE-12-exo, MLE-12 cell-derived exosomes; MLFs, Mouse lung fibroblasts; mRNA-seq, mRNA sequencing; NAT10, N-acetyltransferase 10; NC, negative control; oe, over expression; oeMETTL1/MDR4-TC-1-exo, Exosomes of TC-1 cells overexpressing METTL1/WDR4; PFKFB3, 6-phosphofructo-2-kinase/fructose-2,6-biphosphatase 3; qRT–PCR, Quantitative real-time PCR; RA, Rosmarinic acid; RA+IR, Rosmarinic acid plus irradiation; RA+IR-TC-1/MLE-12-exo, Exosomes derived from RA intervention in irradiated TC-1/MLE-12 cells; Ribo-seq, Polyribosome-bound mRNA sequencing; RILI, Radiation-induced lung injury; RIPF, Radiation-induced pulmonary fibrosis; rRNA, Ribosomal RNA; si, small interfering RNA; SPHK1, Sphingosine kinase 1; TC-1-exo, TC-1 cell-derived exosomes; tRNA, Transfer RNA; tRNA-seq, tRNA sequencing; TE, Translation efficiency; TRs, Translation ratios; UV, Ultraviolet; WT, Wild type.

Data Sharing Statement

The online version contains supplementary material available at GSE249534 (https://www.ncbi.nlm.nih.gov/geo/query/acc.cgi?acc=GSE249534). This study was posted on the preprint server Research Square (https://doi.org/10.21203/rs.3.rs-3744363/v1).

Acknowledgments

We are grateful for the support of the Guangxi Key Laboratory of Immunology and Metabolism for Liver Diseases and the Key Laboratory of Early Prevention and Treatment for Regional High-Frequency Tumors of Guangxi Medical University.

Author Contributions

All authors made meaningful contributions to the work reported, whether in the conception, study design, execution, acquisition of data, analysis and interpretation, or in all these areas; took part in drafting, revising or critically reviewing the article; gave final approval of the version to be published; agreed on the journal to which the article has been submitted; and agreed to be accountable for all aspects of the work.

Funding

This work was supported by the "Medical Excellence Award" Funded by the Creative Research Development Grant from the First Affiliated Hospital of Guangxi Medical University, the Natural Science Foundation of Guangxi Zhuang Autonomous Region (2024GXNSFBA010244), the Basic Ability Enhancement Project of Young Teachers in Guangxi Zhuang Autonomous Region (2023KY0120) and the Nanning Qingxiu district key research and development plan for Science and Technology (2020019).

Disclosure

The authors declare that they have no conflicts of interest in this study.

References

1. He Y, Thummuri D, Zheng G, et al. Cellular senescence and radiation-induced pulmonary fibrosis. *Transl Res*. 2019;209:14–21. doi:10.1016/j.trsl.2019.03.006
2. Liu D, Gong L, Zhu H, et al. Curcumin inhibits transforming growth factor β induced differentiation of mouse lung fibroblasts to myofibroblasts. *Front Pharmacol*. 2016;7:419. doi:10.3389/fphar.2016.00419

3. Guan R, Zhao X, Wang X, et al. Emodin alleviates bleomycin-induced pulmonary fibrosis in rats. *Toxicol Lett*. 2016;262:161–172. doi:10.1016/j.toxlet.2016.10.004
4. Noor S, Mohammad T, Rub MA, et al. Biomedical features and therapeutic potential of rosmarinic acid. *Arch Pharm Res*. 2022;45(4):205–228. doi:10.1007/s12272-022-01378-2
5. Farhadi F, Baradaran Rahimi V, Mohamadi N, et al. Effects of rosmarinic acid, carnosic acid, rosmanol, carnosol, and ursolic acid on the pathogenesis of respiratory diseases. *Biofactors*. 2022;49(3):478–501. doi:10.1002/biof.1929
6. Hsieh YH, Tsai JP, Ting YH, et al. Rosmarinic acid ameliorates renal interstitial fibrosis by inhibiting the phosphorylated-AKT mediated epithelial–mesenchymal transition in vitro and in vivo. *Food Funct*. 2022;13(8):4641–4652. doi:10.1039/d2fo00204c
7. Zhang X, Ma ZG, Yuan YP, et al. Rosmarinic acid attenuates cardiac fibrosis following long-term pressure overload via AMPKα/Smad3 signaling. *Cell Death Dis*. 2018;9(2):102. doi:10.1038/s41419-017-0123-3
8. Zhang T, Liu C, Ma S, et al. Protective effect and mechanism of action of rosmarinic acid on radiation-induced parotid gland injury in rats. *Dose Response*. 2020;18(1):1559325820907782. doi:10.1177/1559325820907782
9. Zhang T, Ma S, Liu C, et al. Rosmarinic acid prevents radiation-induced pulmonary fibrosis through attenuation of ROS/MYPT1/TGFβ1 signaling Via miR-19b-3p. *Dose Response*. 2020;18(4):1559325820968413. doi:10.1177/1559325820968413
10. Li N, Li K, Zhao W, et al. Small extracellular vesicles from irradiated lung epithelial cells promote the activation of fibroblasts in pulmonary fibrosis. *Int J Radiat Biol*. 2023:1–13. doi:10.1080/09553002.2023.2263550
11. Jarzebska N, Karetnikova ES, Markov AG, et al. Scarred lung. an update on radiation-induced pulmonary fibrosis. *Front Med*. 2020;7:585756. doi:10.3389/fmed.2020.585756
12. Chen Z, Fang Y, Zhang S, et al. Haplodeletion of follistatin-like 1 attenuates radiation-induced pulmonary fibrosis in mice. *Int J Radiat Oncol Biol Phys*. 2019;103(1):208–216. doi:10.1016/j.ijrobp.2018.08.035
13. Qian Q, Ma Q, Wang B, et al. Downregulated miR-129-5p expression inhibits rat pulmonary fibrosis by upregulating STAT1 gene expression in macrophages. *Int Immunopharmacol*. 2022;109:108880. doi:10.1016/j.intimp.2022.108880
14. Wang M, Qin Z, Wan J, et al. Tumor-derived exosomes drive pre-metastatic niche formation in lung via modulating CCL1(+) fibroblast and CCR8 (+) Treg cell interactions. *Cancer Immunol Immunother*. 2022;71(11):2717–2730. doi:10.1007/s00262-022-03196-3
15. Chen L, Shi Z, Deng L, et al. Construction of MicroRNA-mRNA regulatory network in the molecular mechanisms of bleomycin-induced pulmonary fibrosis. *Biomed Res Int*. 2022;2022:7367328. doi:10.1155/2022/7367328
16. Chen J, Li K, Chen J, et al. Aberrant translation regulated by METTL1/WDR4-mediated tRNA N7-methylguanosine modification drives head and neck squamous cell carcinoma progression. *Cancer Commun*. 2022;42(3):223–244. doi:10.1002/cac2.12273
17. Ying X, Liu B, Yuan Z, et al. METTL1-m(7) G-EGFR/EFEMP1 axis promotes the bladder cancer development. *Clin Transl Med*. 2021;11(12):e675. doi:10.1002/ctm2.675
18. Han H, Yang C, Ma J, et al. N(7)-methylguanosine tRNA modification promotes esophageal squamous cell carcinoma tumorigenesis via the RPTOR/ULK1/autophagy axis. *Nat Commun*. 2022;13(1):1478. doi:10.1038/s41467-022-29125-7
19. Zhang H, Zhou Y, Wen D, et al. Noncoding RNAs: master regulator of fibroblast to myofibroblast transition in fibrosis. *Int J Mol Sci*. 2023;24(2). doi:10.3390/ijms24021801
20. Cui W, Zhao D, Jiang J, et al. tRNA modifications and modifying enzymes in disease, the potential therapeutic targets. *Int J Biol Sci*. 2023;19(4):1146–1162. doi:10.7150/ijbs.80233
21. Vangaveti S, Ranganathan SV, Agris PF. Agris PF physical chemistry of a single tRNA-modified nucleoside regulates decoding of the synonymous lysine wobble codon and affects type 2 diabetes. *J Phys Chem B*. 2022;126(6):1168–1177. doi:10.1021/acs.jpcb.1c09053
22. Shen L, Gan M, Tan Z, et al. A novel class of tRNA-derived small non-coding RNAs respond to myocardial hypertrophy and contribute to intergenerational inheritance. *Biomolecules*. 2018;8(3):54. doi:10.3390/biom8030054
23. Huang LS, Sudhadevi T, Fu P, et al. Sphingosine Kinase 1/S1P signaling contributes to pulmonary fibrosis by Activating Hippo/YAP pathway and mitochondrial reactive oxygen species in lung fibroblasts. *Int J Mol Sci*. 2020;21(6). doi:10.3390/ijms21062064
24. Ye Q, Zhou Y, Zhao C, et al. Salidroside Inhibits CCl(4)-induced liver fibrosis in mice by reducing activation and migration of HSC Induced by liver sinusoidal endothelial cell-derived exosomal SphK1. *Front Pharmacol*. 2021;12:677810. doi:10.3389/fphar.2021.677810
25. Piñuela C, Baatrup E, Geneser F. Geneser FA Histochemical distribution of zinc in the brain of the rainbow trout, Oncorhynchus myciss. II. The diencephalon. *Anat Embryol*. 1992;186(3):275–284. doi:10.1007/bf00174150
26. Shenshen W, Yin L, Han K, et al. NAT10 accelerates pulmonary fibrosis through N4-acetylated TGFB1-initiated epithelial-to-mesenchymal transition upon ambient fine particulate matter exposure. *Environ Pollut*. 2023;322:121149. doi:10.1016/j.envpol.2023.121149
27. Xie N, Tan Z, Banerjee S, et al. Glycolytic Reprogramming in Myofibroblast Differentiation and Lung Fibrosis. *Am J Respir Crit Care Med*. 2015;192(12):1462–1474. doi:10.1164/rccm.201504-0780OC
28. Xiong Y, Guan KL. Mechanistic insights into the regulation of metabolic enzymes by acetylation. *J Cell Biol*. 2012;198(2):155–164. doi:10.1083/jcb.201202056
29. Jiang A, Liu J, Wang Y, et al. cGAS-STING signaling pathway promotes hypoxia-induced renal fibrosis by regulating PFKFB3-mediated glycolysis. *Free Radic Biol Med*. 2023;208:516–529. doi:10.1016/j.freeradbiomed.2023.09.011
30. Yang Q, Huo E, Cai Y, et al. PFKFB3-mediated glycolysis boosts fibroblast activation and subsequent kidney fibrosis. *Cells*. 2023;12(16):2081. doi:10.3390/cells12162081
31. Wang F, Yin X, Fan YM, et al. Upregulation of glycolytic enzyme PFKFB3 by deubiquitinase OTUD4 promotes cardiac fibrosis post myocardial infarction. *J Mol Med*. 2023;101(6):743–756. doi:10.1007/s00109-023-02323-6
32. Liu HY, Liu YY, Yang F, et al. Acetylation of MORC2 by NAT10 regulates cell-cycle checkpoint control and resistance to DNA-damaging chemotherapy and radiotherapy in breast cancer. *Nucleic Acids Res*. 2020;48(7):3638–3656. doi:10.1093/nar/gkaa130
33. Li FL, Liu JP, Bao RX, et al. Acetylation accumulates PFKFB3 in cytoplasm to promote glycolysis and protects cells from cisplatin-induced apoptosis. *Nat Commun*. 2018;9(1):508. doi:10.1038/s41467-018-02950-5
34. Yalcin A, Clem BF, Simmons A, et al. Nuclear targeting of 6-phosphofructo-2-kinase (PFKFB3) increases proliferation via cyclin-dependent kinases. *J Biol Chem*. 2009;284(36):24223–24232. doi:10.1074/jbc.M109.016816
35. Marsin AS, Bouzin C, Bertrand L, et al. The stimulation of glycolysis by hypoxia in activated monocytes is mediated by AMP-activated protein kinase and inducible 6-phosphofructo-2-kinase. *J Biol Chem*. 2002;277(34):30778–30783. doi:10.1074/jbc.M205213200

36. Huang R, Hao C, Wang D, et al. SPP1 derived from silica-exposed macrophage exosomes triggers fibroblast transdifferentiation. *Toxicol Appl Pharmacol*. 2021;422:115559. doi:10.1016/j.taap.2021.115559
37. Li Y, Zhang J, Shi J, et al. Exosomes derived from human adipose mesenchymal stem cells attenuate hypertrophic scar fibrosis by miR-192-5p/IL-17RA/Smad axis. *Stem Cell Res Ther*. 2021;12(1):221. doi:10.1186/s13287-021-02290-0
38. Zeyada MS, Eraky SM, El-Shishtawy MM. El-Shishtawy MM Trigonelline mitigates bleomycin-induced pulmonary inflammation and fibrosis: insight into NLRP3 inflammasome and SPHK1/S1P/Hippo signaling modulation. *Life Sci*. 2024;336:122272. doi:10.1016/j.lfs.2023.122272
39. Cheresh P, Kim SJ, Huang LS, et al. The sphingosine kinase 1 inhibitor, PF543, mitigates pulmonary fibrosis by reducing lung epithelial cell mtDNA damage and recruitment of fibrogenic monocytes. *Int J Mol Sci*. 2020;21(16):5595. doi:10.3390/ijms21165595
40. Zheng J, Tan Y, Liu X, et al. NAT10 regulates mitotic cell fate by acetylating Eg5 to control bipolar spindle assembly and chromosome segregation. *Cell Death Differ*. 2022;29(4):846–860. doi:10.1038/s41418-021-00899-5
41. Xu S, Cheuk YC, Jia Y, et al. Bone marrow mesenchymal stem cell-derived exosomal miR-21a-5p alleviates renal fibrosis by attenuating glycolysis by targeting PFKM. *Cell Death Dis*. 2022;13(10):876. doi:10.1038/s41419-022-05305-7
42. Ding H, Jiang L, Xu J, et al. Inhibiting aerobic glycolysis suppresses renal interstitial fibroblast activation and renal fibrosis. *Am J Physiol Renal Physiol*. 2017;313(3):F561–f575. doi:10.1152/ajprenal.00036.2017
43. De Bock K, Georgiadou M, Schoors S, et al. Role of PFKFB3-driven glycolysis in vessel sprouting. *Cell*. 2013;154(3):651–663. doi:10.1016/j.cell.2013.06.037
44. Luo W, Tao Y, Chen S, et al. Rosmarinic acid ameliorates pulmonary ischemia/reperfusion injury by activating the PI3K/Akt signaling pathway. *Front Pharmacol*. 2022;13:860944. doi:10.3389/fphar.2022.860944
45. Ma L, Liu C, Zhao Y, et al. Anti-pulmonary fibrosis activity analysis of methyl rosmarinate obtained from Salvia castanea Diels f. tomentosa Stib. using a scalable process. *Front Pharmacol*. 2024;15:1374669. doi:10.3389/fphar.2024.1374669
46. Bahri S, Mies F, Ben Ali R, et al. Rosmarinic acid potentiates carnosic acid induced apoptosis in lung fibroblasts. *PLoS One*. 2017;12(9):e0184368. doi:10.1371/journal.pone.0184368
47. Wang Q, Liu J, Hu Y, et al. Local administration of liposomal-based Srpx2 gene therapy reverses pulmonary fibrosis by blockading fibroblast-to-myofibroblast transition. *Theranostics*. 2021;11(14):7110–7125. doi:10.7150/thno.61085
48. Chang CJ, Lin CF, Lee CH, et al. Overcoming interferon (IFN)-γ resistance ameliorates transforming growth factor (TGF)-β-mediated lung fibroblast-to-myofibroblast transition and bleomycin-induced pulmonary fibrosis. *Biochem Pharmacol*. 2021;183:114356. doi:10.1016/j.bcp.2020.114356
49. Zhang JX, Huang PJ, Wang DP, et al. m(6)A modification regulates lung fibroblast-to-myofibroblast transition through modulating KCNH6 mRNA translation. *Mol Ther*. 2021;29(12):3436–3448. doi:10.1016/j.ymthe.2021.06.008